Quark Matter '96
Heidelberg, Germany
May 20-24, 1996

BNL-63430

CONF-960579--4

Particle Production in Au + Au collisions from BNL E866

Y. Akiba, for the E802 Collaboration

BNL-UCBerkeley-UCRiverside-Columbia-INS(Tokyo)-Kyoto-LLNL-Maryland-MIT-Tokyo-Tsukuba-Yonsei

L.Ahle[8], Y.Akiba[5], K.Ashktorab[1], M.D.Baker[8], D.Beavis[1], H.C.Britt[7], J.Chang[3], C.Chasman[1], Z.Chen[1], C.-Y.Chi[4], Y.Y.Chu[1], V.Cianciolo[8], B.A.Cole[4], H.J.Crawford[2], J.B.Cumming[1], R.Debbe[1], J.C.Dunlop[8], W.Eldredge[3], J.Engelage[2], S.-Y.Fung[3], E.Garcia[12], M.Gonin[1], S.Gushue[1], H.Hamagaki[5], R.S.Hayano[9], S.Hayashi[10], G.Heintzelman[8], S.Homma[5], E.Judd[2], H.Kaneko[6], J.Kang[11], E.-J.Kim[11], A.Kumagai[10], K.Kurita[10], J.-H.Lee[1], M.J.Levine[1], J.Luke[7], Y.Miake[10], A.Mignerey[12], B.Moskowitz[1], M.Moulson[4], C. Muentz[1], S.Nagamiya[4], M.N.Namboodiri[7], C.Ogilvie[8], J.Olness[1], L.P.Remsberg[1], H.Sako[5], T.C.Sangster[7], R.Seto[3], J.Shea[12], K.Shigaki[9], R.Soltz[7], S.G.Steadman[8], G.S.F.Stephans[8], M.J.Tannenbaum[1], J.H.Thomas[7], F.Videbæk[1], F.Wang[4], Y.Wang[4], Y.Wu[4], H.Xiang[3], G.H.Xu[3], K.Yagi[10], X.Yang[4], H. Yao[8], W.A.Zajc[4], Q.Zhu[3], F.Zhu[1]

[1] Brookhaven National Laboratory, Upton, NY 11973
[2] University of California, Space Sciences Laboratory, Berkeley, CA 94720
[3] University of California, Riverside, CA 92507
[4] Columbia University, New York, NY 10027 and Nevis Laboratories, Irvington, NY 10533
[5] Institute for Nuclear Study, University of Tokyo, Tokyo 188, Japan
[6] Kyoto University, Sakyo-ku, Kyoto 606, Japan
[7] Lawrence Livermore National Laboratory, Livermore, CA 94550
[8] Massachusetts Institute of Technology, Cambridge, MA 02139
[9] Department of Physics, University of Tokyo, Tokyo 113, Japan
[10] University of Tsukuba, Tsukuba, Ibaraki 305, Japan
[11] Yonsei University, Seoul 120-749, Korea
[12] University of Maryland,College Park, MD 20742

Recent single-particle measurements from the AGS E866 experiment are presented. The transverse mass distributions and rapidity distributions of p, $\pi^{\pm}$, $K^{\pm}$, and $\overline{p}$ in Au+Au central collisions as well as their centrality dependence are shown.

1. Introduction

In this article, we present recent results on particle production from Au+Au collisions at 11 A GeV/c obtained by the E866 experiment. The experiment studies the particle production in high baryon density matter created in central Au + Au collisions. Preliminary

nary results of proton and pion production have been reported in previous Quark Matter conferences[1–4]. Two particle correlation data for Au+Au collisions in this experiment are presented in another paper in this conference[5].

2. Experimental Setup

The experiment consists of several subsystems. A schematic diagram of the experimental apparatus was described elsewhere[3]. Here we briefly describe the subsystems that are used for the measurements in this article.

Beam line counters select Au beam particles, and provide the minimum bias (INT) trigger by measuring the dE/dx of the beam particle before and after the target. The INT trigger was required in all more selective triggers and in all data in this article. The measured cross section of the INT trigger (σ_{INT}) is about 5.3 barn, which is smaller than the total cross section of Au+Au ($\sim$ 6.8 barn)[8]. The zero degree calorimeter (ZCAL) measures the total energy of beam fragments, and it provides a measure of the centrality of the collision. Two magnetic spectrometers placed on opposite sides of the beam line measure the charged particles from the reaction. An array of δE-E telescopes (PHOS) measures p, d, t from target fragments.

One of the spectrometers, the Henry Higgins spectrometer (HH), has been used in E802/E859 for measurement in p+A, O+A, and Si+A reactions (see, e.g. [6]). In the Au+Au data in this article, it was used to cover angles larger than 21 degrees in the laboratory frame. The smaller spectrometer, the Forward Spectrometer (FS), was built for the Au beam experiment[7]. It has a relatively small solid angle ($\sim$ 5 msr), but is equipped with a better tracking system to cope with the high particle density from Au+Au reactions. The spectrometer measures particle production from 6 degrees to $\sim$ 28 degrees in the laboratory frame using several angle settings. Both spectrometers are equipped with finely segmented, high resolution Time-of-Flight counters to identity particle species. The average TOF resolution in the FS is about 75 ps r.m.s., while it is about 100 ps in the HH.

The FS covers forward rapidity ($y \geq y_{cm} - 0.2$) for pions, and mid-rapidity ($|y - y_{cm}| \leq 0.6$) for kaons and protons, where $y_{cm} = 1.6$ is the c.m.s. rapidity of the colliding nuclei. The HH covers the backward rapidity region down to $y - y_{cm} \sim -1.0$ for pions and to $y - y_{cm} \sim -1.2$ for kaons and protons. By using both spectrometers, the experiment can measure identified charged particle spectra in a wide interval of rapidity and transverse momentum. In addition, there is a reasonable overlap between the two spectrometers. This provides a good test of systematic uncertainties of the data. The PHOS detector extends the measurement of protons to the target rapidity region.

We took Au+Au collision data from 1992 through 1995. In 1992, we have data only from the HH (HH92). In 1993, the FS was commissioned while the HH took data. In 1994 and 1995, both spectrometer were operational. We present here the results of data analysis of the HH92, the HH93, and the FS94 data sets.

There is a small difference in beam energy among the data sets. The beam momentum in the AGS was 11.45 A GeV/c in 1992, 11.09 A GeV/c in 1993, and 11.67 A GeV/c in 1994 and 1995[9]. The effect of beam energy difference is not corrected for in the data presented in this article.

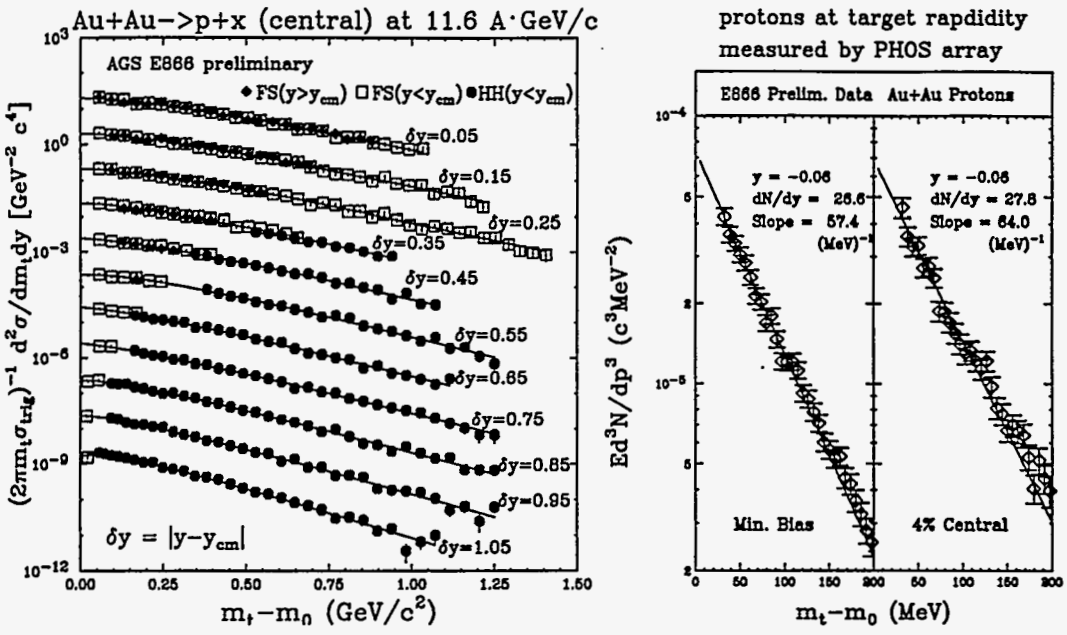

Figure 1. Left: Invariant yield $1/\sigma_{trig} E d^2\sigma/dp^3$ of protons from central (7%) Au+Au collisions at 11.6 A GeV/c in rapidity bins of width 0.1 at average rapidity $\delta y = |y - y_{cm}|$. The topmost spectrum ($\delta y = 0.05$) is absolutely normalized, while each successive spectrum is divided by 10. Right: Invariant yield of protons at target rapidity measured by the PHOS array. The data are shown for minimum bias events and for central (4 %) events.

3. Particle Production in central Au+Au collisions

3.1. Proton spectra

Figure 1 shows transverse mass spectra of protons from central Au+Au collisions. The transverse mass, m_t, is defined as $m_t = \sqrt{p_t^2 + m_0^2}$, where p_t is the transverse momentum and m_0 is the rest mass. The data correspond to the most central 370 mb of Au+Au collisions selected by the energy measurement in ZCAL. This is about 7 % of σ_{INT} (5.3 barn) and about 5.5 % of geometrical total cross section ($\sim$ 6.8 barn). The data shown are the HH92 data at larger angles ($\theta \geq 24$ degrees) and the FS94 data in the forward angles. Since the spectra should be symmetric around y_{cm}, they are plotted in $\delta y = |y - y_{cm}|$. The FS data in ($y > y_{cm}$), in ($y < y_{cm}$), and the HH data in the same δy and m_t agree reasonably well.

For p+A and light ion (^{16}O and ^{28}Si) collisions, the transverse mass spectra are well described by a single exponential form in m_t. In central Au+Au collisions, the proton spectra deviate from single exponential shape at low m_t. The spectra become less steep and the deviation from the single exponential is more pronounced near mid-rapidity. Although the spectra near mid-rapidity are not well described by a single exponential, we would obtain an inverse slope parameter T of 250 to 300 MeV if a single exponential fit was used. Those values are higher than those observed in central Si+Al collisions (T

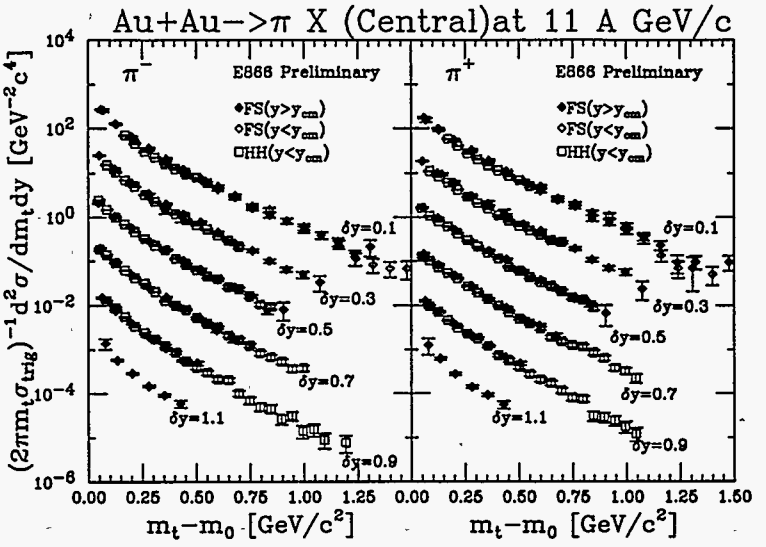

Figure 2. Invariant yield of $\pi^{\pm}$ from central Au+Au collisions at 11 A GeV/c in different rapidity bins ($\delta y = |y - y_{cm}|$). The topmost spectrum ($\delta y = 0.1$) is absolutely normalized, while each successive spectrum is divided by 10. The data from the Forward Spectrometer are plotted in diamonds, while the data from the Henry Higgins Spectrometer are plotted in squares.

$\sim$ 250 MeV)[11]. We use a double exponential form to fit the proton spectrum as

$$1/\sigma_{trig} E d^2\sigma/dp^3 = A_1 \exp(-m_t/T_0) + A_2 \exp(-m_t/T_1), \quad (1)$$

where A_1, A_2, T_0, T_1 are fitting parameters. The results of the fit are shown in the figure as solid curves.

The right panels of figure 1 show the m_t distribution of protons at target rapidity ($|y - y_{cm}| = 1.66$). Here the spectrum is well described by a single exponential form. When compared with the spectra in mid-rapidity, the spectrum is much steeper, with inverse slope of about 60 MeV. It is also noted that the rapidity density is almost unchanged from minimum bias events to central events in the target rapidity region.

3.2. Pion Spectra

Figure 2 shows the transverse mass spectra of pions from central Au+Au collisions. In the figure, data from the FS in ($y > y_{cm}$) and the data from the HH in ($y < y_{cm}$) are overlapped in the same δy bins. The data from the two spectrometers agree within systematic errors of 10 %.

Contrary to the proton spectra, which show a suppression at low m_t, the pion spectra are enhanced at low m_t, and they also cannot be well described by a single exponential form. The difference between the pion and the proton spectra can be more easily seen in figure 3. The proton spectrum deviates downward from single exponential while π^+ and π^- spectra deviate upwards. The enhancement at low m_t is larger for π^- than π^+. As a

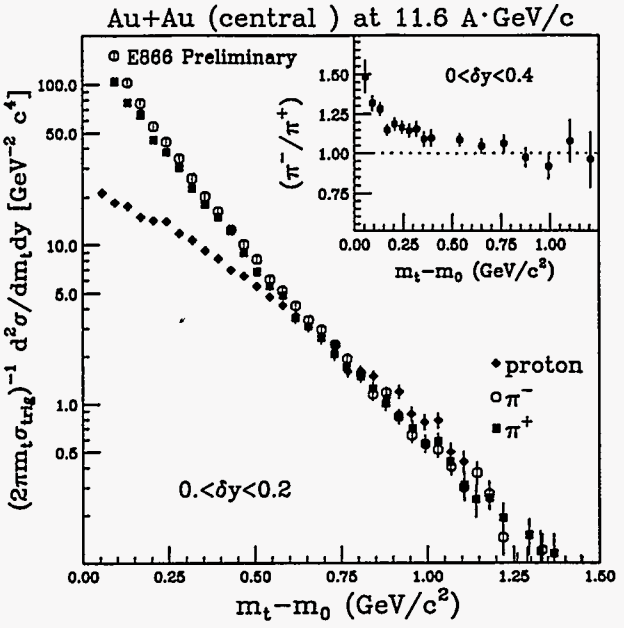

Figure 3. The m_t distributions of p and $\pi^{\pm}$ in central rapidity ($|y - y_{cm}| < 0.2$). The insert shows the yield ratio of π^-/π^+.

result, the ratio π^-/π^+ becomes larger for small m_t, as shown in the insert of the figure. At low m_t, the π^-/π^+ratio is about 1.5 and it gradually decreases with m_t, approaching unity in the high m_t region.

There are several possible explanations for the low m_t enhancement of π^-. Since Au nuclei have a larger number of neutrons than protons, the baryon resonances such as Δ produced in Au+Au collisions would produce more π^- than π^+. Since the momentum of pion from resonance decay is relatively small, more π^- than π^+ are expected at low m_t. Weak decay of $\Lambda \rightarrow \pi^- p$ also tends to produce low momentum π^-, and some of the π^-'s from Λ decay are accepted due to limited target resolution of the spectrometers. Coulomb forces from the positively charged co-moving nuclear matter would also enhance the π^-/π^+ratio at low m_t. In fact, the observed π^-/π^+ratio could be reproduced by the Gamow correction factor[3]. However, this is a static calculation, and more detailed dynamical calculations are required to quantitatively evaluate the effect.

3.3. Kaon spectra

Strange particle production has been considered as an important probe of nucleus-nucleus collisions since the enhancement of strangeness is a potential signature of the QGP. Strangeness production is also a measure of the chemical equilibration achieved in the collision. The data from the E802 show that the production of kaons is enhanced in Si+A collisions compared with p+p and p+A[10,11]. It is important to extend these kaon measurements to Au+Au collisions.

Figure 4 shows the m_t spectra of K^+ and K^- in central Au + Au collisions. The

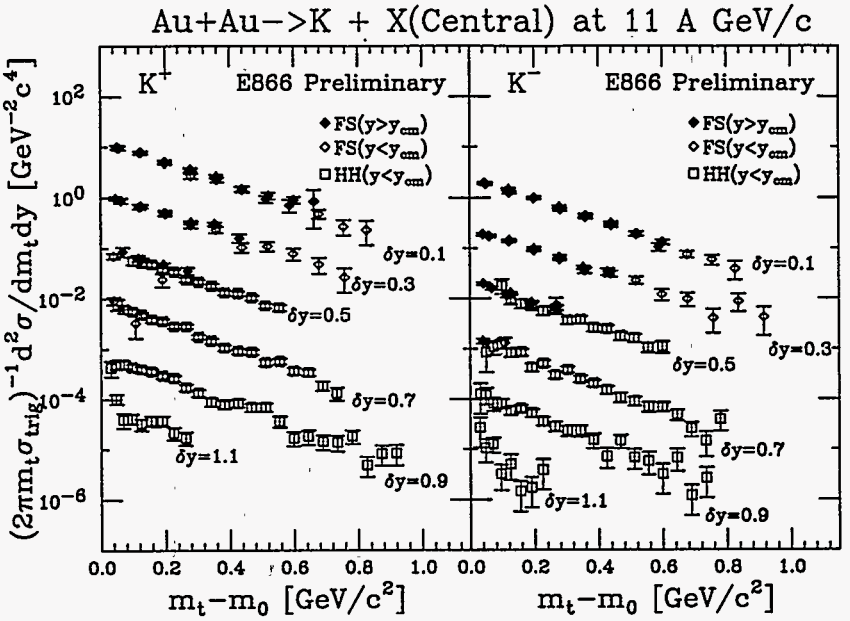

Figure 4. The m_t distributions of $K^{\pm}$ from central Au+Au collisions at 11 A GeV/c in different rapidity bins ($\delta y = |y - y_{cm}|$). Starting with $\delta y = 0.1$ at the top, each successive spectrum is divided by 10.

figure shows the FS94 data in central rapidity region ($|y - y_{cm}| \leq 0.6$) and the HH93 data in large rapidity ($|y - y_{cm}| \geq 0.4$). The spectra are well described by a single exponential form, and the inverse slope parameters are 170 to 200 MeV for both K^+ and K^-. Those values are similar to those observed in Si+A collisions.

There is a small difference in energy in the data from the two spectrometers. The beam momentum of the FS94 data is 11.67 A GeV/c, while it is 11.09 A GeV/c in the HH93 data. The production cross section $p + p \rightarrow K^+(K^-)X$ has a steep beam energy dependence. The cross section increases from $p_{beam} = 12$ GeV/c to 24 GeV/c by a factor of 2 for K^+, and by 4.5 for K^-[12]. Therefore, the 6 % difference in energy could produce a difference of kaon yield in the two data sets. From the beam energy dependence of kaon production in p+p[13,14], we estimate that the increase of the yield would be about 6 % for K^+, and 15 to 20 % for K^-. This effect is not corrected in the data.

3.4. Anti-proton spectra

Measurement of anti-protons in nucleus-nucleus collisions at the AGS is interesting for several reasons. Because of their large absorption cross section in nuclear matter, anti-protons could possibly be used to probe baryon density reached in the collision. Since the beam energy is very close to the nucleon-nucleon threshold, multi-step processes can play a large role in $\overline{p}$ production. However, the observed $\overline{p}$ production is a product of the competing processes of initial production and annihilation in nuclear matter. It is therefore very important to measure the production over a wide kinematic range to

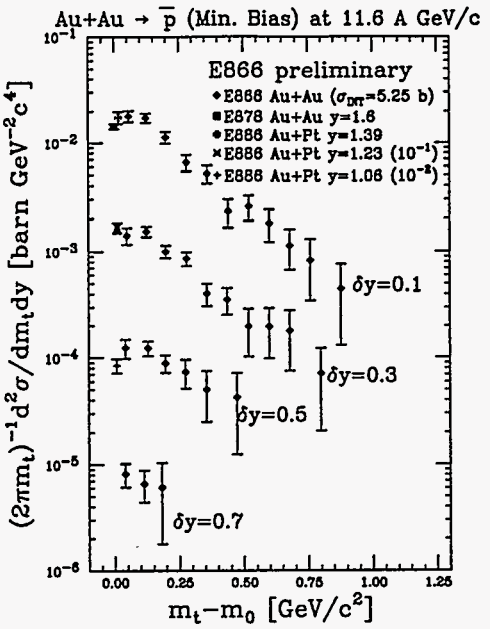

Figure 5. Invariant cross section of $\overline{p}$ from Au+Au collisions at 11.6 A GeV/c in different rapidity bins ($\delta y = |y - y_{cm}|$). The topmost spectrum is absolutely normalized, while each successive spectrum is divided by 10. Data from other experiments in Au+Au collisions at the AGS are also shown.

decipher those processes.

From 15 million spectrometer triggers in the FS94 data, we collected about 800 $\overline{p}$'s in the central rapidity region. The $\overline{p}$'s are identified by the TOF in $p_{lab} \leq 4.5$ GeV/c. Because of the finite resolution of the TOF system, there is a small background from K^- and π^- in the identified $\overline{p}$ sample. The background contamination is estimated by a double Gaussian fit to the observed m^2 distribution from TOF in each momentum bins. The background is 0 to 25 %, and it is subtracted from the data.

Figure 5 shows the invariant production cross section of $\overline{p}$'s from Au+Au collisions. Since σ_{INT} (5.25 barn) is smaller than the geometrical cross section (6.8 barn), the $\overline{p}$'s produced in the most peripheral Au+Au collision could be lost by the trigger bias. We studied the centrality dependence of $\overline{p}$ yield in our data, and estimated that the loss by the INT trigger was about 8 %. The loss was corrected as a constant normalization factor in the data in figure 5. The figure also shows the $\overline{p}$ cross section near $m_t - m_0 = 0$ measured by E878[15] and E886[16]. Our data are consistent with their data, and we extend the $\overline{p}$ measurement to larger values of m_t, up to $m_t - m_0 \sim 1$ GeV. The spectra are well described by a single exponential, and the inverse slope parameter is about 250 MeV. A cascade model calculation of nucleus-nucleus collision predicts that strong $\overline{p}$ absorption causes a suppression in low m_t[17]. There is a hint of such suppression in our data, but with the present statistics, it is not significant.

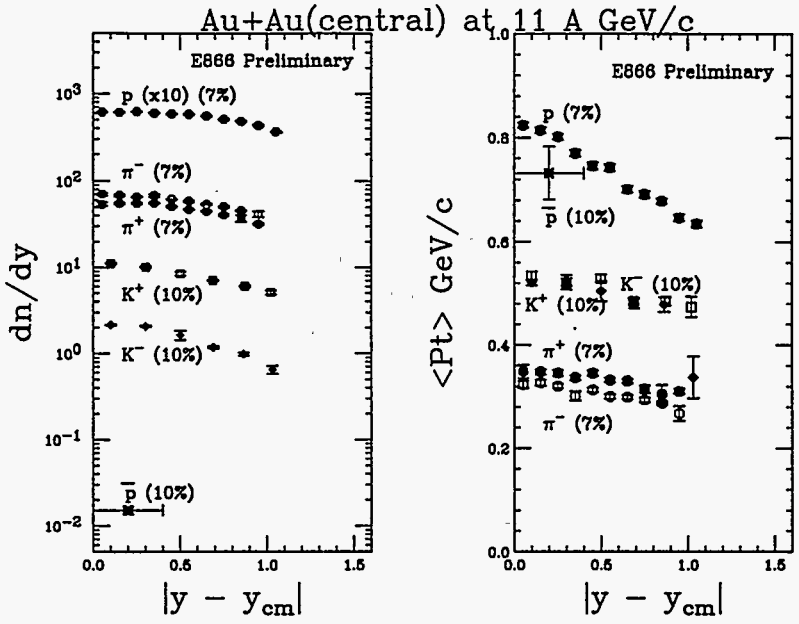

Figure 6. Left: Rapidity density dn/dy of p, $\pi^{\pm}$, $K^{\pm}$, and $\overline{p}$ in central Au + Au collisions. The points for protons are multiplied by 10 to avoid the overlap with pions. Right: Average transverse momentum of p, $\pi^{\pm}$, $K^{\pm}$, and $\overline{p}$ as function of rapidity.

3.5. Rapidity distributions and average transverse momentum

Figure 6 shows the rapidity density dn/dy and average transverse momentum $< p_t >$ of p, $\pi^{\pm}$, $K^{\pm}$, and $\overline{p}$ in central Au+Au collisions. For p+A and light ion collisions, we have used a single exponential fit to the m_t spectra to obtain dn/dy and the inverse slope parameter T. However, as we observed in the previous section, this parameterization is not adequate for p and $\pi^{\pm}$ in Au+Au collisions. We used the double exponential function to obtain dn/dy and $< p_t >$ for p and $\pi^{\pm}$. For $K^{\pm}$ and $\overline{p}$, a single exponential fit was used.

For p and $\pi^{\pm}$, the data from two spectrometers (the FS94 data set and the HH92 data set) are combined in the fit. The beam energy of the two data sets are similar, and the chi-squares of the fit show that the two data sets are consistent. For $K^{\pm}$, the data points in $|y - y_{cm}| \leq 0.4$ are from the FS94, the points in $|y - y_{cm}| > 0.6$ are from the HH93, and the points at $|y - y_{cm}| = 0.5$ are the average of the two measurements. The rapidity distribution of pions and kaons are well described by a Gaussian shape, with $\sigma_y^{\pi} \sim 0.9$, $\sigma_y^{K^+} \sim 0.8$, and $\sigma_y^{K^-} \sim 0.7$. Since K^- production has a very steep beam energy dependence, the narrower rapidity distribution of K^- could be partly attributed to the 6% energy difference of mid-rapidity points (at 11.67A GeV/c) and large rapidity points (at 11.09 A GeV/c).

The dn/dy of p, $\pi^{\pm}$, and $K^{\pm}$ have maximum at mid-rapidity, and the maximum values of dn/dy are about 60 for p, 70 for π^-, 55 for π^+, 11 for K^+, and 2.2 for K^-, respectively.

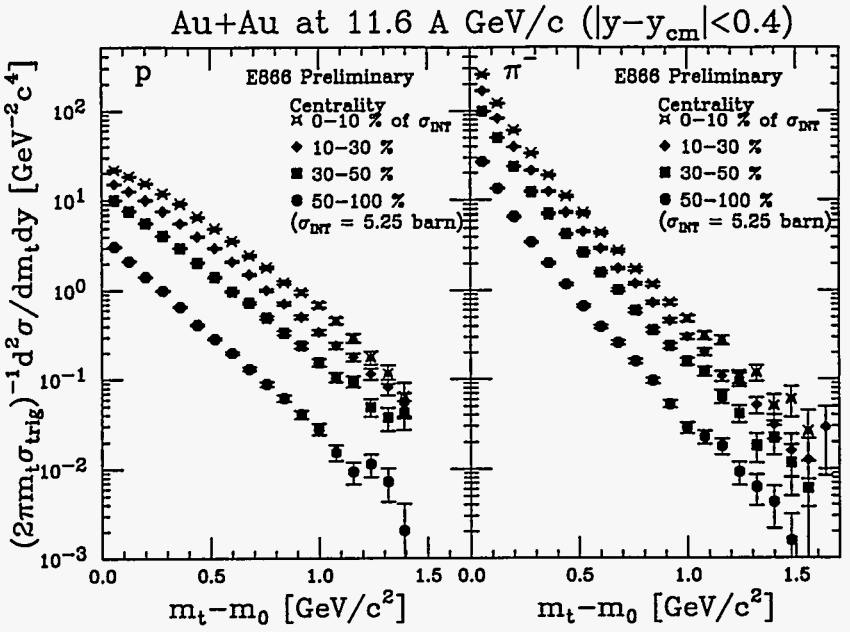

Figure 7. The m_t spectra of protons and π^- in four centrality bins (central 10 %, 10-30 %, 30-50 %, and most peripheral 50 - 100 % of $\sigma_{INT} = 5.25$ barn).

Because of limited acceptance and small statistics, we obtained only the average dn/dy of $\overline{p}$ in $|y - y_{cm}| \leq 0.4$, and it is about 0.015. The errors shown in the figure are the statistical ones only, and there is an additional over-all normalization uncertainty of 10 to 15 %.

There is a broad maximum in the proton dn/dy at the c.m.s. rapidity. This is consistent with a large baryon stopping power at the AGS energy. The difference of dn/dy between π^- and π^+could be caused by isospin effects. The K^+/π^+ratio at mid-rapidity, about 20 %, is similar to the value reached in Si+Au collisions[11].

The average p_t of p, $\pi^{\pm}$, $K^{\pm}$, and $\overline{p}$ are plotted in the right panel of figure 6. There is a large rapidity dependence of $< p_t >$ for protons. It decreases from about 0.8 GeV/c at $|y - y_{cm}|$=0 to 0.6 GeV/c at $|y - y_{cm}|$=1. The $< p_t >$ of kaons and pions also decreases for larger δy, but the change is much smaller. For $\overline{p}$, we do not have enough statistics to see the rapidity dependence. The $< p_t >$ of $\overline{p}$ is similar to that of p, although with a very large statistical error.

4. Centrality dependence of particle production

4.1. m_t distributions

Figure 7 shows the m_t spectra of p and π^- in mid-rapidity ($|y - y_{cm}| \leq 0.4$) in four centrality bins (10 %, 10 to 30 % , 30 to 50 %, and 50 to 100 % of σ_{INT}). The centrality is selected by the energy in ZCAL.

There is an interesting difference in the centrality dependence of π^- and p. The shape

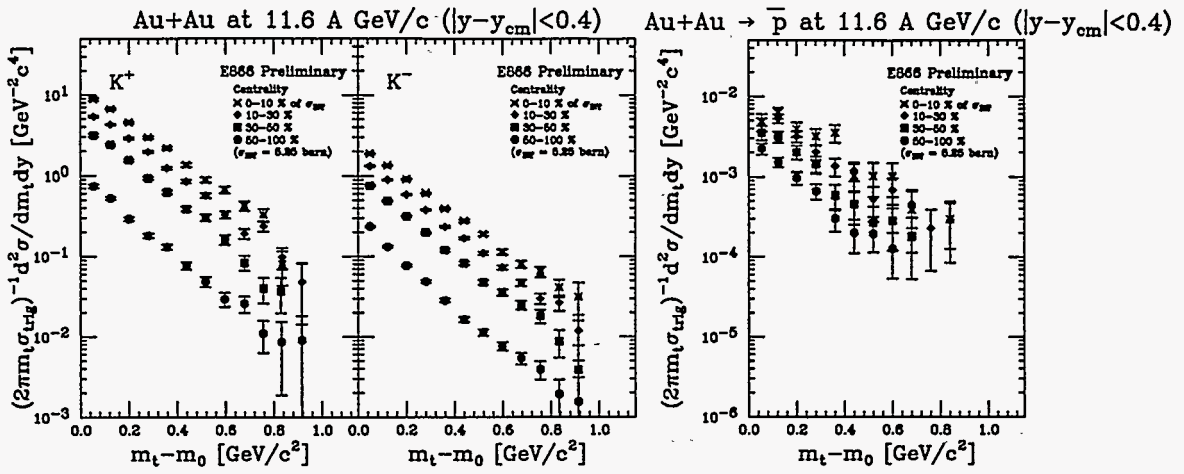

Figure 8. Centrality dependence of m_t spectra of K^+, K^-, and $\overline{p}$.

of the π^- spectrum is almost unchanged as the centrality increases. On the other hand, we see a dramatic change in the shape of the m_t spectrum of protons. The spectrum is well described by a single exponential in the most peripheral bin, but the distribution becomes flatter, and the suppression at low m_t becomes more pronounced, as the centrality increases.

The left side panels of figure 8 shows the m_t spectra of K^+ and K^- in the same four centrality bins. Similar to the π^- spectra, the shapes of kaon spectra are almost unchanged with centrality. The ratios of the yields in the different centrality bins are larger in kaons than in pions. This means that the kaon yield increases more rapidly than the pion yield as the centrality increases. The right side panel of the figure shows the centrality dependence of the $\overline{p}$ m_t distribution. While statistics are not sufficient to discuss quantitatively the change of the spectrum shape with centrality, we note that the change in yield between the $\overline{p}$ spectra for different centrality bins are much smaller than that for the kaons and pions. This means that the $\overline{p}$ yield increases very slowly with centrality. A possible interpretation of this phenomena is the absorption of $\overline{p}$ in co-moving nuclear matter.

4.2. Rapidity distributions

Figure 9 shows the rapidity distribution of p, π^-, K^+, and K^- in the same four centrality bins. For protons, the rapidity density at the target rapidity ($|y - y_{cm}| = 1.66$) measured by the PHOS detector in central and minimum bias events are also plotted. Similar to the transverse mass distribution, the largest change with centrality is observed for protons. For all other particles, the dn/dy distribution have Gaussian-like shapes in all centrality bins, and the shapes are almost unchanged by the centrality. On the other hand, the proton dn/dy shows a large centrality dependence. In the peripheral collision, the proton dn/dy has a peak at target rapidity, with a valley in the mid-rapidity. While the observed rapidity density in the target rapidity is almost unchanged, the density at

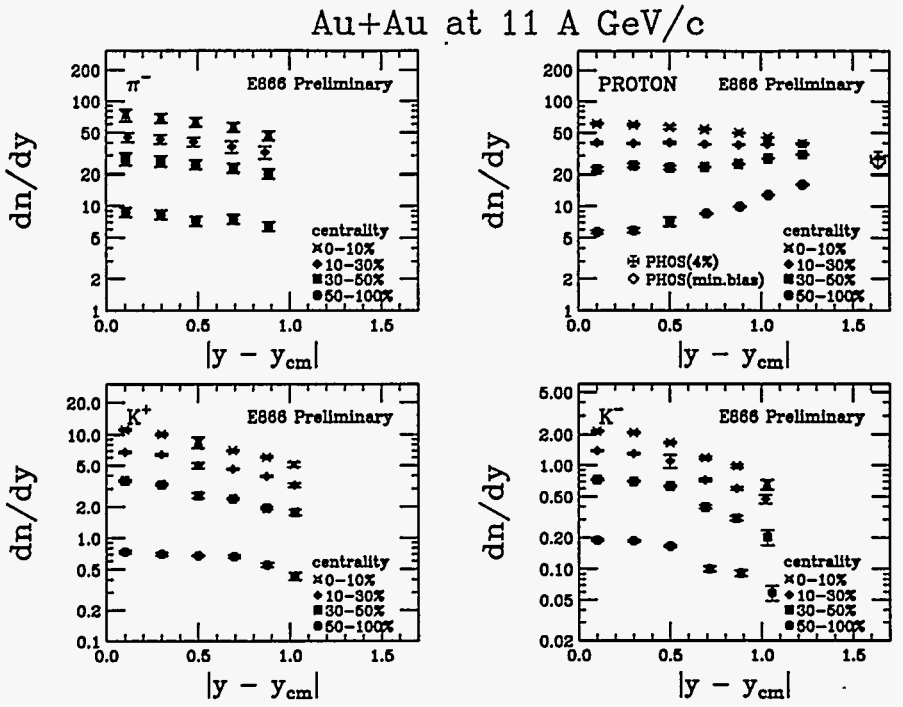

Figure 9. Rapidity distributions of π^-, p, K^+, and K^- in four centrality bins (central 10%, 10-30 %, 30-50 %, and 50-100 %). The top-right panel for proton also shows dn/dy in minimum bias and central 4 % collisions measured by the PHOS detector.

the mid-rapidity increases very rapidly as the centrality increases. In the most central bin, the distribution has a maximum at mid-rapidity. This illustrates the large stopping of baryons in the Au+Au collisions at the AGS energy.

4.3. Particle yield and $< m_t >$ in mid-rapidity

In the left panel of figure 10, the relative dn/dy of charged hadrons (p, $\pi^{\pm}$, $K^{\pm}$, $\overline{p}$) at mid-rapidity ($|y - y_{cm}| \leq 0.4$) are plotted as a function of the number of projectile participants, N_{pp}. The dn/dy of all particles are normalized to the most peripheral centrality bin to show the relative increase of the yields.

There are several ways to estimate N_{pp} from the total energy measured in ZCAL. One way is to directly convert the energy to N_{pp} according to

$$N_{pp} = A_p(1 - E_{ZCAL}/E_{beam}), \tag{2}$$

where $A_p(= 197)$ is the mass number of the projectile, E_{beam} is the total kinetic energy of the beam, and E_{ZCAL} is the energy measured in ZCAL. Another way, which is employed in this figure, is to convert the centrality (an interval of cross section) to the corresponding interval of impact parameter b from the relation $\sigma = \pi b^2$, and then to estimate N_{pp} in the impact parameter interval by a geometrical model of a nucleus-nucleus collision. The two estimates of N_{pp} agree within 5 to 10 % for mid-central to central collisions. However,

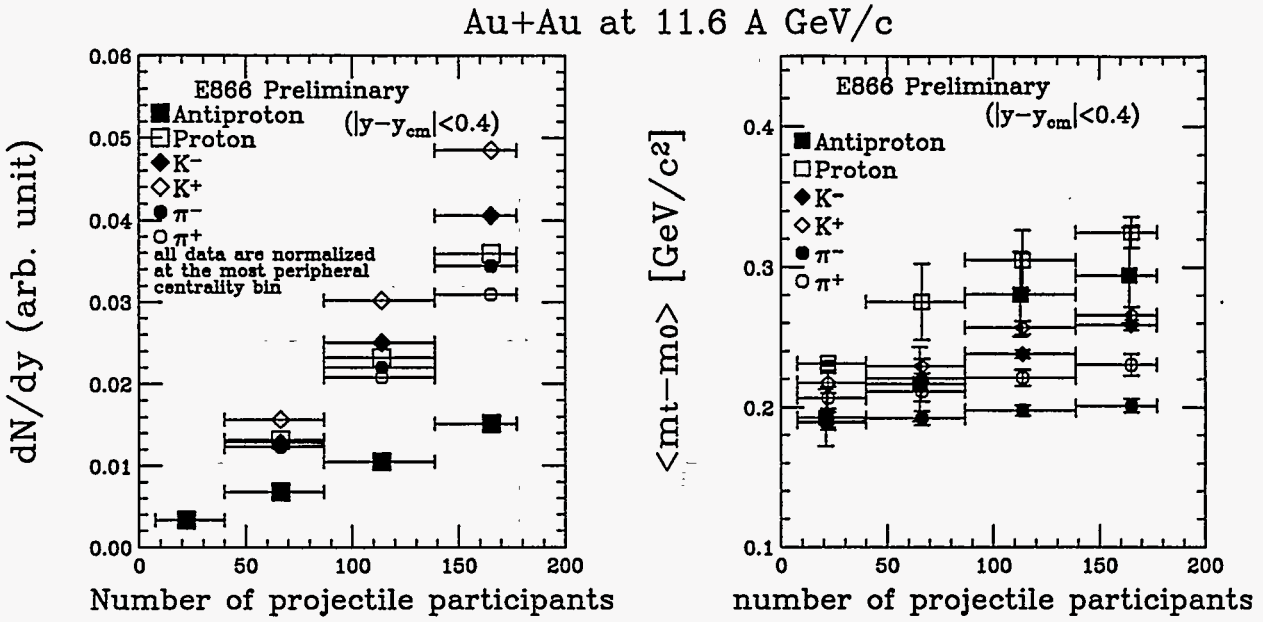

Figure 10. Rapidity density of p, π^-, K^+, K^-, and $\overline{p}$ in mid-rapidity ($|y - y_{cm}| \leq 0.4$) in four centrality bins (10%, 10-30%, 30-50%, and 50-100%.) The dn/dy values of all particles are normalized to the value in the most peripheral bin. The abscissa shows estimated values of the number of projectile participant in the centrality bins. The right panel shows the mean $m_t - m_0$ of p, $\pi^{\pm}$, $K^{\pm}$, and $\overline{p}$ in the same centrality bins.

for the most peripheral centrality bins, the two values are different by more than 20 %, which is mostly caused by the energy calibration uncertainty in ZCAL in the 94 data.

It is observed that the dn/dy of kaons increases most rapidly with the centrality. In this figure, it appears as if kaon yield increases non-linearly with N_{pp}. However, since there is systematic uncertainty in the estimate of N_{pp}, some caution is required. The increase in the dn/dy of pions is smaller, and it is consistent with a linear increase with N_{pp} over this range of N_{pp}. The increase of $\overline{p}$ yield with centrality is much suppressed compared with other particles. This suggests that absorption of $\overline{p}$ in nuclear matter plays a major role in the $\overline{p}$ production in Au+Au collision.

The right panel of figure 10 shows the average transverse kinetic energy $m_t - m_0$ of p, $\pi^{\pm}$, $K^{\pm}$, and $\overline{p}$ as function of N_{pp}. It is seen that the transverse mass of all particles increases with centrality. The increase is largest for protons, followed by $\overline{p}$, $K^{\pm}$, and $\pi^{\pm}$ in order. It is interesting that the order is the same as the order of the mass of the particle. This behavior is consistent with a picture of a (nearly) thermalized hadronic gas with radial expansion. In such a picture, heavier particles receive larger $< m_t >$ due to radial expansion.

4.4. Particle ratios

Figure 11 shows the ratios of particle yield at mid-rapidity in the four centrality bins. It

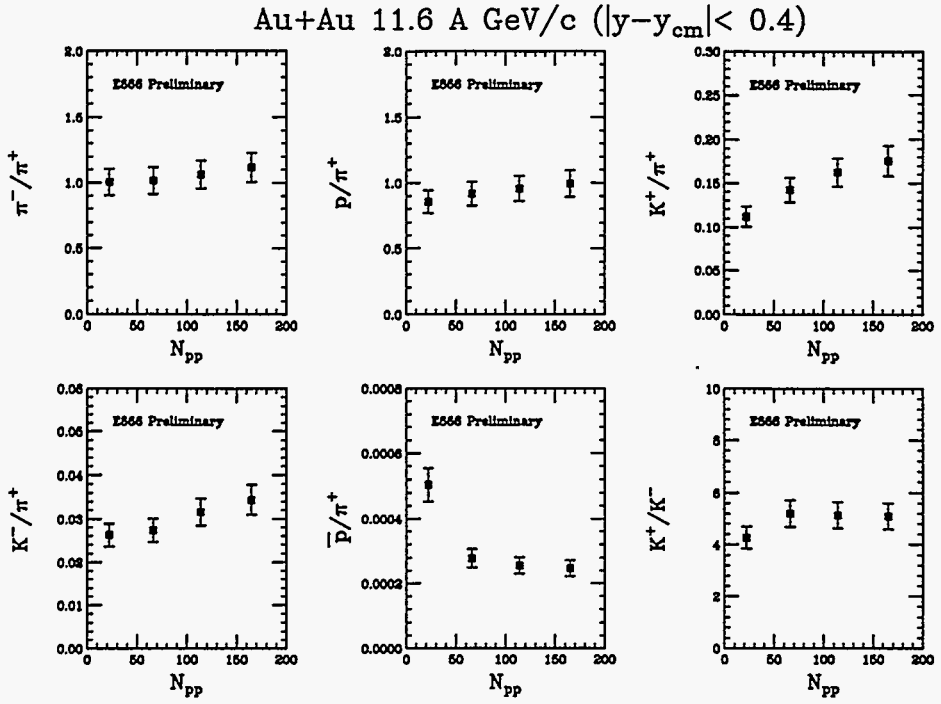

Figure 11. Particle ratios π^-/π^+, p/π^+, K^-/π^+, K^+/π^+, $\overline{p}/\pi^+$, and K^+/K^- at mid-rapidity as function of centrality.

is observed that the ratios $\pi^+/\pi^-$and p/π^+ are almost unchanged, while the K^+/π^+ and the K^-/π^- ratios increase with centrality. There is a large drop in the $\overline{p}/\pi^+$ ratio from peripheral collisions to the central collisions. The increase of kaon yield suggests that multiple interactions and rescattering play a large role in kaon/strangeness production in nucleus-nucleus collisions. The K^+/π^+ratio reaches about 18%, which is similar to the value reached in Si+Au collisions. The K^+/K^- ratio, $\sim$ 5, is somewhat larger than the value in Si+A collisions ($\sim$ 4.0). However, this difference can well be attributed to the beam energy difference. The drop of the $\overline{p}$ yield relative to other particles can be interpreted as an indication of strong annihilation of $\overline{p}$ in dense matter created in the collision.

5. Summary

In summary, we measured single particle distributions from Au+Au collisions at the AGS. In central Au+Au collisions, we have the following observations:

1. The proton dn/dy distribution has a maximum plateau at mid-rapidity. This indicates a large baryon stopping.

2. The mean p_t of protons has a strong rapidity dependence. It has a maximum at mid-rapidity.

3. The pion m_t spectra have an enhancement at low m_t. The enhancement is larger for π^- than π^+. The π^-/π^+ ratio reaches to 1.5 in mid-rapidity near $m_t - m_0 = 0$. This effect could be explained by baryon resonances such as Δ's, by Λ decay, and by Coulomb interaction with co-moving protons.

4. The mean p_t of particles are in the order $p \sim \overline{p} > K^{\pm} > \pi^{\pm}$

For centrality dependence of particle production, we observed:

1. The m_t distributions of protons becomes flatter, and $< m_t > (p)$ increases with centrality. The changes in m_t spectral shape and $< m_t >$ are much smaller for all other particles.

2. Changes in $< m_t >$ with centrality are in the order of $p > \overline{p} > K^{\pm} > \pi^{\pm}$. This is the same as the order of the rest mass of particles.

3. The kaon yield increases faster with centrality than pions. The maximum value of the K^+/π^+ ratio, 18 ± 2 %, is similar to the value observed in Si+Au collisions.

4. the increase of $\overline{p}$ yield with centrality is much slower than pions. This could be a consequence of $\overline{p}$ absorption in co-moving baryons.

This work is supported by the U.S. Department of Energy under contracts with BNL, Columbia University, LLNL, MIT, UC Riverside, by NASA under contract with University of California, by the Ministry of Education and KOSEF in Korea, and by the Ministry of Education, Science and Culture of Japan under Japan-US agreement on cooperation in High Energy Physics.

REFERENCES

1. H. Hamagaki, Nucl. Phys. A566 (1994) 27c.
2. M. Gonin, Nucl. Phys. A566 (1994) 601c.
3. F. Videbaek, et. al., Nucl. Phys. A590 (1995) 249c.
4. K. Shigaki, Nucl. Phys. A590 (1995) 519c.
5. M.D.Baker, et. al., these proceedings.
6. T. Abbott, et. al., Nucl. Inst. Meth. A290 (1990) 41.
7. Details of the Forward Spectrometer is in K. Shigaki, Ph.D thesis, U. Tokyo (1995) and H. Sako, Ph.D thesis, U. Tokyo (1996).
8. Estimated from T.F. Hoang, et. al., Z. Phys. C29 (1985) 611.
9. P. Pile, private communication.
10. T. Abbott et al., Phys. Rev. Lett. 64 (1990) 847.
11. T. Abbott et al., Phys. Rev. C50 (1994) 1024.
12. H. Fesfeldt, et. al, Nucl. Phys. B147 (1979) 317.
13. A. M. Rossi, et. al., Nucl. Phys. B84 (1975) 269.
14. M. Antinucci, et. al., Nouv Cim. Lett. 6 (1973) 121.
15. D. Beavis, et al. (E878 collaboration), Phys. Rev. Lett. 75 (1995) 3633.
16. G. E. Diebold, et al. (E886 collaboration), Phys. Rev. C48 (1993) 2984.
17. A Jahns, et al., Nucl. Phys. A566 (1994) 483c.